Additive manufacturing of high density pure tungsten by electron beam melting

D. Dorow-Gerspach[1], A. Kirchner[2], Th. Loewenhoff[1], G. Pintsuk[1], T. Weißgärber[2], M. Wirtz[1]

[1] Forschungszentrum Jülich, Institut für Energie- und Klimaforschung - Plasmaphysik, 52425 Jülich, Germany

[2] Fraunhofer Institute for Manufacturing Technology and Advanced Materials (IFAM), 01277 Dresden, Germany

Abstract

Tungsten is an outstanding material and due to its properties like highest melting point and tensile strength of all natural metals and its high thermal conductivity it is a prime candidate for being used in very harsh environments and for challenging applications like X-ray tubes or as plasma facing material (PFM) in fusion reactors. Unfortunately, high brittle to ductile transition temperature and hardness represent a great challenge for classic manufacturing processes. Additive manufacturing (AM) of tungsten could overcome these limitations and resulting design restrictions. However, AM of tungsten also poses challenges in particular related to the production of material of high density and mechanical stability. Using a selective electron beam melting and a base temperature of 1000 °C of the powder, we were able to produce tungsten with a theoretical density of 99 % without the need of any post-treatment like a second melting step or hot isostatic pressing (HIP). The surface morphology, microstructure, hardness, thermal conductivity and stability against severe transient heat loads were investigated with respect to the relevant building parameters and compared with recrystallized standard W. Besides simple test geometries also more sophisticated ones like monoblocks were successfully realized illustrating the potential of AM for fusion.

Introduction

Tungsten (W) is used in a variety of applications benefiting from its unique properties like highest melting point (3420 °C) and lowest vapor pressure of all metals, high thermal conductivity (174 W/mK at 25 °C), strength and chemical resistance [1]. Among other things, because of these properties it is the main candidate for the plasma facing material (PFM) in thermonuclear fusion reactors [2] and other applications where the material has to withstand very high thermal loads at low erosion rates, like rocket nozzles [3] or anodes for X-ray tubes [4]. However, the machinability of W is very poor and thus costly and opposes the possibility of exploiting alternative more sophisticated and complex design solutions for plasma facing components.

With the help of additive manufacturing (AM) some of these design restrictions could be overcome and completely new concepts could be realized. AM, originating from rapid prototyping, has made much progress in the last years and is meanwhile a well-known term, describing typically a layer-by-layer computer-controlled production process in order to generate a three-dimensional object. It thereby offers much more design freedom, for instance the possibility to use topology optimization routines and realize the designs without new molds, machining steps etc. and thus additional costs. In addition, the rapid solidification can lead to a very fine microstructure and the layer-by-layer

approach to inherent texture which both can be influenced by varying the building parameters and, thus, allow the realization of unique microstructures.

For metals the main technique is selective laser melting also called laser powder bed fusion. It is based on a powder bed with or without preheating, a laser as energy source, a powder feeder system and a moveable building platform. In the last years several groups have worked on SLM of tungsten. It turned out that the high melting temperature, high viscosity, thermal conductivity and sensitivity to oxidation make tungsten hard to process with SLM and relative densities of above 80 % are already quite hard to achieve [5, 6]. More recently W with densities of 96 % [7] could be produced by using spherical powder and by increasing the preheating to 1000 °C even 98 % [8] have been reached. However, these dense W samples produced by SLM exhibit a high crack density throughout the whole material, which of course reduces the mechanical stability and usability of the material and it was stated that cracking is almost inevitable in SLM [9].

In this study we used selective electron beam melting (SEBM) instead, which has in principle a similar setup but uses an electron beam as energy source and is thus restricted to conductive materials [10]. SEBM works under vacuum condition, which is very advantageous in the case of W, and high beam powers with extremely high scan speeds up to 10^5 m/s are available, whereas the galvanometric scanners in SLM can reach only about 10 m/s [8]. This allows nearly instantaneous point-to-point jumps and very sophisticated beam patterns including intermediate heating in order to reduce the temperature gradients and evolving stresses.

The aim of this work is to study the effect of the building parameters on the resulting morphology, microstructure and hardness and to find a suitable process window for SEBM of W. In addition, the potential to use such a SEBM tungsten as PFM in a fusion reactor is investigated by applying relevant stationary and transient heat loads and analyze the damage behavior in comparison to recrystallized W (manufactured according to ITER specifications by Plansee SE).

Experimental

Examining the mentioned articles on SLM of W, a consistent result is that spherical powder is necessary to achieve dense W. The used W-powder was supplied by Tekna Advanced Materials Inc. (Quebec, Canada) with a purity of 99.99 wt%, an oxygen content of 0.003 wt%, a tap density (ASTM-B527) of 11.6 and more than 90 wt% of the particles have a diameter between 45 µm and 90 µm. This is considerably larger than the sizes used for SLM, where the median is usually about 25 µm [7, 11, 12].

SEBM processing of W was performed on an Arcam A2X machine using a custom build tank and the standard rake system. Before starting a build procedure, the process chamber was evacuated down to 10^4 mbar or lower. During the build process a helium partial pressure of 2×10^3 mbar was used. A 75 mm x 75 mm steel base plate was used as substrate. Upon raking a powder layer of 50 µm thickness was applied, which was preheated using a defocused electron beam resulting in a base temperature of the powder of 1000 °C. The scan pattern for melting consisted of parallel lines with 100 µm distance (hatch) using a e-beam focus of about 300 µm. After each layer, the scan direction was rotated by 90°.

The main building parameters which have been kept constant, are listed in table 1. In particular the 1000 °C base temperature has been chosen as this is well above the regime in which the brittle-ductile transition temperature (BDTT) of W is situated but below the recrystallization temperature regime of 1200 °C – 1600 °C. By doing so, the stresses generated by the fast solidification process can be relieved but the microstructure produced by AM is not altered to much.

Density of test specimens was established using Archimedes' principle by weighing in air and in water. For metallographic preparation, specimens were cut in build direction, embedded, and polished. High-resolution SEM images (7 MPixel, back scatter contrast) of the surfaces were taken and analyzed with the open source software ImageJ 1.52v, which allows a semi-automated determination of optical density, crack length etc. Dividing this crack length, for which the same magnification and resolution is always used, by the analyzed area (always about 5 mm²), a characteristic crack density [1/m] is calculated.

Table 1: Building parameters which have been kept constant for all samples described in this study.

Base temperature	1000 °C
Substrate material	steel
e-beam focus	~ 300 µm
Layer thickness	50 µm
Hatch distance	100 µm
Particle size	45-90 µm

Table 2: Regime in which power P and scan velocity v of the e-beam have been variied and the resulting line energies. Parameters which resulted in the highest relative density of 99.5 % is given as well.

	P [W]	v [mm/s]	Line energy [J/m]
min	180	144	333
max	1500	1500	5000
Best set	900	180	5000

As mentioned before, one application for W is as armor at the inner wall in a fusion reactor. A critical aspect for such a PFM is its behavior under high heat flux (HHF) loadings of several MW/m² stationary (including cyclic ramp up and cool down) and transient in the order of GW/m² on a ms time scale, originating from plasma edge instabilities [2]. For these tests, bulk samples of 12x12x5mm³ were prepared out of the SEBM-W and in addition a reference sample which was conventionally produced W (manufactured according to ITER specifications by Plansee SE) and recrystallized at 1600 °C for 1 h. The reason for this reference was that no mechanical after treatment like forging etc. was employed and as the powder is melted during AM, it is expected that the mechanical properties will be most comparable with the recrystallized state. All samples were grinded and polished to a mirror like surface finish and brazed on actively cooled Cu holders using an Ag-Cu braze allowing the efficient removal of applied heat and therefore a higher frequency during the thermal shock loading tests. The electron beam facility JUDITH 2, located at Forschungszentrum Jülich, was used for these tests [13] using specially developed loading patterns for the application of high pulse number transient thermal loads at high frequency [14]. For the cooling a water temperature of 70 °C, a pressure of 20 MPa and a flow velocity of about 25 ms^{-1} was employed. A stationary heat load of 10 MW/m² has been applied on all samples in order to achieve a surface temperature of about 700 °C prior to the transients. The samples surface temperature was monitored using an IR camera (ImageIR® 8380 from InfraTec GmbH). A high number of 10^5 pulses with 0.14 GW/m² for 0.48 ms with a repetition frequency of 25 Hz was applied as transient heat load. The total number of pulses were divided in ten blocks, with a 20 s break in between, allowing the component to cool down completely and thus simulating 10 on/off cycles. Typically, the sample cool down behavior from 700 °C to 300 °C (lower temperatures were below the threshold of the measurable range of the IR camera) follows a classic exponential decay with time constants between

100 ms and 150 ms. This rapid cool down could in principle lead to a shattering of AM-W because of the existing cracks and residual stress within the material.

Results

The top surfaces were examined after the building was completed and in figure 1 images of 4x4 mm² large parts of the surfaces are shown. It is well known that the scan speed v and the power of the beam P are the two main parameters effecting the result in terms of powder sintering, melting or boiling/splashing and thus the obtainable density. Therefore, the line energy $E_L = P/v$ is a useful parameter, especially when hatch distance and layer thickness are not altered like in our study [10, 12, 15].
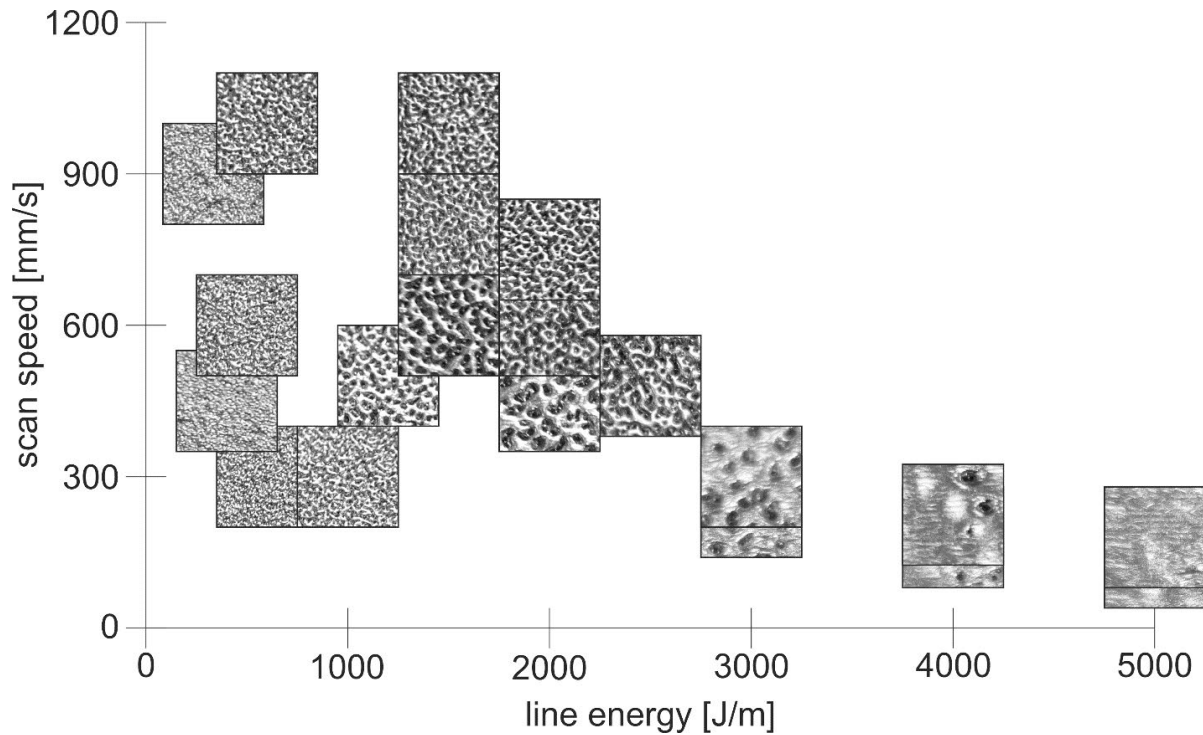
Figure 1: Surface images of the samples in the as built state. Higher line energies result in a transition from particle sintering via partial melting to complete melting of the powder. In addition, it can be noticed that higher scanning velocities lead to slightly finer surface morphologies even for constant line energies.

The surfaces depicted in figure 1 are illustrating the transition from particle sintering via partial melting to complete melting of the surface and reduction of residual pores with increasing line energy as expected. What is interesting to note here is that even for the same line energy higher velocities have a large impact on the surface morphology resulting in slightly finer structures in the transition region between powder sintering and melting.

This transition can be clearly identified by surface roughness (R_a) measurements, for which results obtained by using a laser profilometer (KF3 sensor from OPM Messtechnik GmbH) are shown in figure 2. At low line energies the consolidation of the powder is governed by sintering and the particle sizes of the powder determine the obtained roughness of about 30 µm. At higher line energies partial melting is achieved; however, the tendency of W for balling [6, 16] due to its high surface tension increases the obtained roughness. Higher line energies increase the molten volume

and also the temperature of the melt, leading to a more and more flattened surface and at the highest line energy a minimum R_a value of 1.5 µm was obtained.
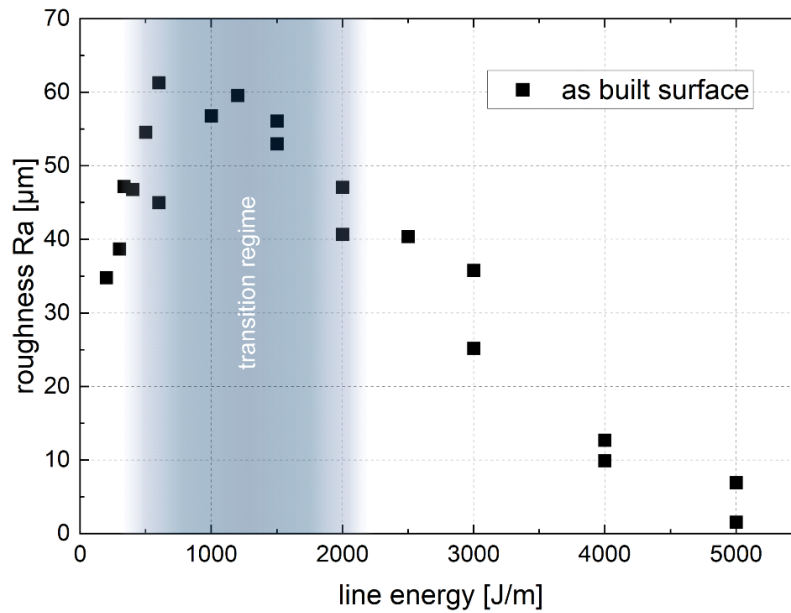

Figure 2: Surface roughness R_a of the as built state measured by laser profilometry. Transition from pure sintering, partially melting (increased roughness due to balling) and finally complete surface melting causing a reduction of surface roughness with increasing line energy can be seen.

For the further investigations we have focused on the high line energies of and above 3000 J/m, as, based on the results so far, no material with suitable quality and density can be expected below.

The relative density of these samples is shown in figure 3, which are all above 96 % with a maximum of 99.5 %. However, the line energy alone is not sufficient to explain the evolving densities and quality of SEBM-W, as it was also the case for the as built surfaces shown in figure 1. For every line energy, the higher beam power results in a higher density. Most profoundly, this effect can be seen when looking at the 900 W, 4000 J/m sample which has not only a significant higher density than its 720 W counterpart but also than the 720 W, 5000 J/m one.
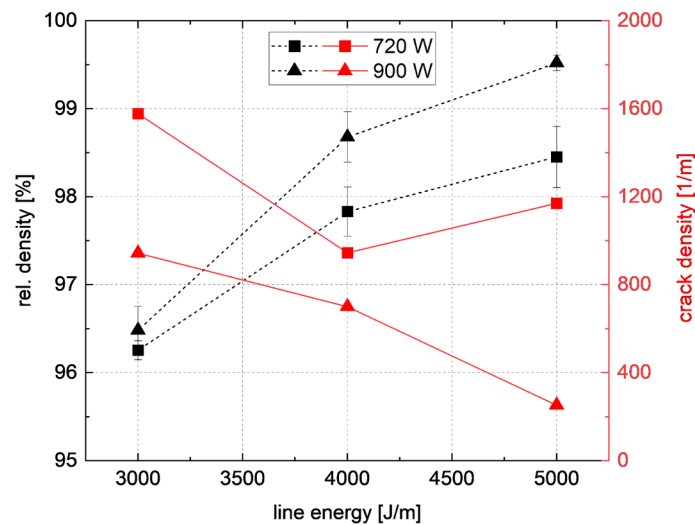

Figure 3: Relative density (Archimedes principle) and crack density (crack length/area) at the polished surface of the SEBM-W in the as-built state. Increasing the line energy improves the quality (higher density and fewer cracks), interestingly, an additional dependence on the beam intensity or scan speed respectively can be seen here, as it was indicated before.

In figure 3 also the crack density is shown. The absolute value itself has only a limited meaning as it depends to some degree on the details of the analyzation procedure and magnification. However, as the same semi-automatic procedure is employed on similar images it allows a quantified comparison of the material quality or damage behavior. Here, the general trend is that a higher material density correlates with a lower crack density. This result is encouraging although it was not fully obvious as, also very porous samples can be crack free, because the open volume reduces the evolving thermal stresses during the manufacturing process. However, they are not suitable as PFM due to their inferior mechanical strength and thermal conductivity. In addition, similar to material density, the beneficial effect of higher beam power even with the same line energy is also observed for the crack density allowing a clear identification of the best manufacturing parameters and the path to further optimization.

Both phenomena, less cracks and higher density with higher beam power, can be attributed to the extraordinary high thermal conductivity of W. Strictly speaking, the concept of line energy is valid only if the thermal response of the material is much slower than the scan speed. The over proportional influence of the beam power suggests that this assumption is not true in this case, and that the energy of the beam dissipates already partly during the exposure. Thus, a low beam power cannot be fully compensated by a slow scanning, which explains the difference in the resulting AM-W built by SLM and SEBM.

In a next step, test cubes were cut along the building direction to analyze the microstructure within the material and light microscope images are shown in figure 4. Despite the very high, Archimedes, density of all samples, the cutting reveals that not all powder is fully molten and firmly bond to the surrounding material, leading to the removal of particles during the grinding/polishing process. For instance, this results in a higher optical pore density of about 7 – 10 % in figure 4a compared to 3.7 % determined by Archimedes principle. By increasing the line energy and in particular power this effect vanishes almost completely, as shown in figure 4f where the optical pore density is about 0.7 %, which is practically the same as the 0.5 % determined via Archimedes principle.
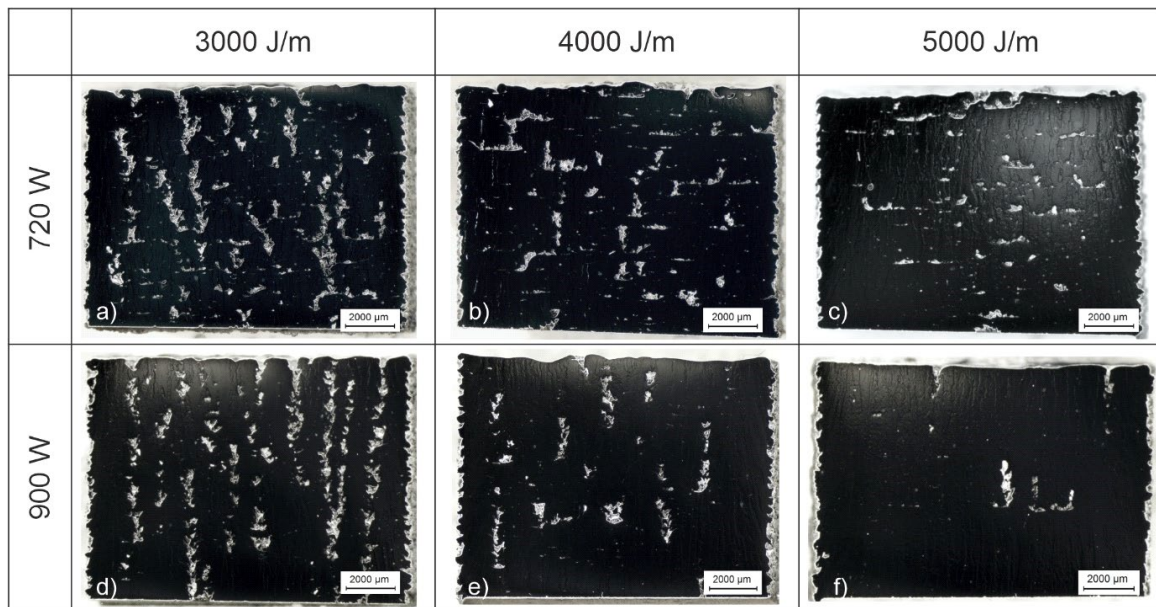

Figure 4: Microscope images of the cross section of the samples in the as-built state, manufactured with the three highest line energies used in this study. With the highest line energy and power, W with nearly no pores or unmelted particles, could be produced.

To get further insight in the evolving microstructure of SEBM-W and differences to recrystallized W, EBSD (electron backscatter diffraction) measurements have been performed at cross sections. Some

exemplary results are shown in figure 5. Columnar grain structure was observed similar to those obtained for SLM-W [9, 12], which is a result of the typical layer-by-layer procedure used in AM [10].
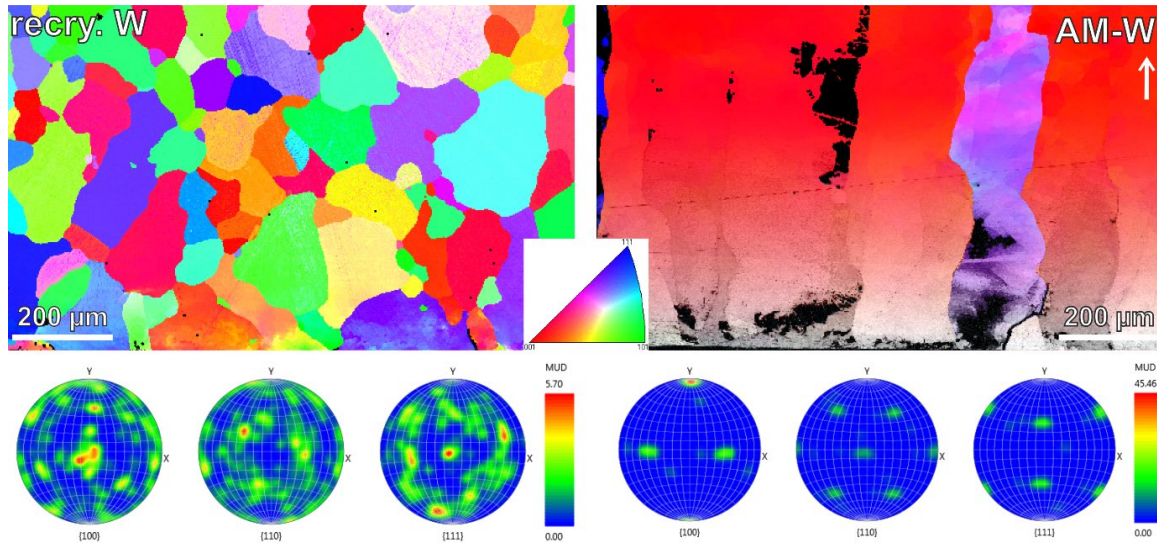

Figure 5: EBSD analysis, orientation with respect to the building direction which is indicated by the arrow, and pole-figures of recrystallized and SEBM-W using the best parameter set (table 2). For better detectability of the columnar grain structure (width 100-200 μm) which is observed in SEBM-W, a band contrast overlay is shown at the lower half of the image. Interestingly, the grains have also a strong texture, whereas a complete random distribution is present for the recrystallized reference W.

Moreover, these columnar grains, with a width of 100-200 μm, are not randomly oriented as for example in recrystallized W but exhibit a strong 100 texture in the building direction, which was not reported in previous studies. The same was observed for the SEBM-W built with only 4000 J/m, illustrating that this phenomenon can be observed also at somewhat lower energies, thus melt pool temperatures. It's worth noting that steel was employed as building platform and not for instance a W single crystal.
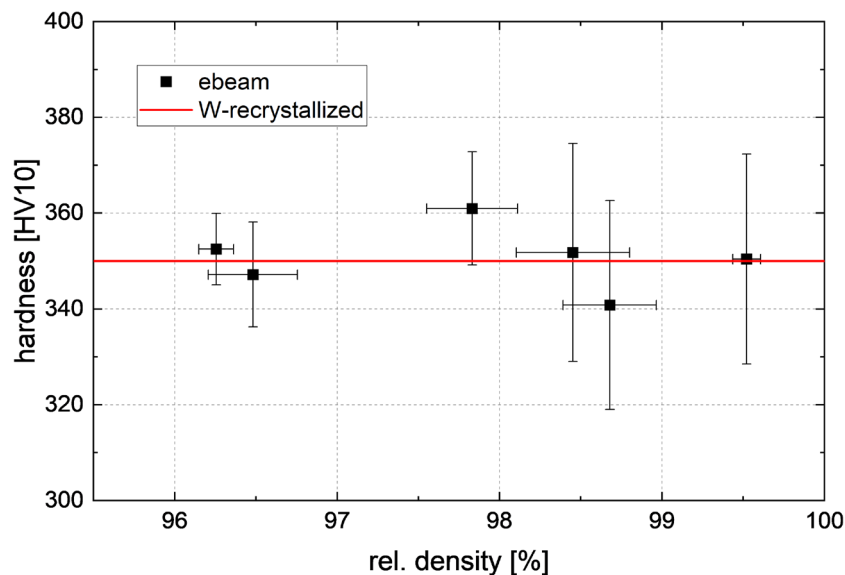

Figure 6: Hardness (HV 10) of polished surfaces versus their density determined by Archimedes principle. No correlation for these high-density W samples can be seen and their mean value is equal to recrystallized tungsten [Alfonson2015]. Only these high-density SEBM-W samples were loaded in JUDITH 2.

After bars (13x13x25 mm³) were built by SEBM, they have been cut perpendicular to the building direction to produce the different samples for the experiments. Hardness was measured along such a sectional plane, thus within the bulk of the material, being at about 350 HV10 for all measured materials, which corresponds to the hardness of recrystallized W in contrast to 430 HV10 of deformed W [17]. No significant variation in hardness was found within the plane, which demonstrates the sufficient homogeneity of the SEBM-W as well as no correlation between density and hardness was observed (see figure 6). The low value similar to recrystallized W is a result of the low dislocation density, which is increased in industrially manufactured materials by mechanical deformation techniques like forging or rolling and were not applied after the solidification / printing process in this study.

High heat flux (HHF) loading

Figure 7 exemplarily shows the IR thermogram of the SEBM-W built by 720 W and a line energy of 4000 J/m under 10 MW/m² stationary heat load. Figure 7a) illustrates the homogeneity of the evolving surface temperature and with a mean value of about 700 °C, which indicates a similar heat handling capability and correlated thermal conductivity as known from standard W. After applying 10^5 transients with 0.14 GW/m² on top of the stationary heat load, the evolving surface temperature during the end-screening, shown in figure 7b), appears slightly hotter, in particular in the central area. This increase can mainly be attributed to an increased emissivity at the point of impact due to surface modifications caused by the transients with their limited spot size [14], which is a known phenomenon also for standard W. The near-edge area has still the same temperature as in the beginning, indicating the structural stability despite the cracks that are still present within the material after the SEBM.
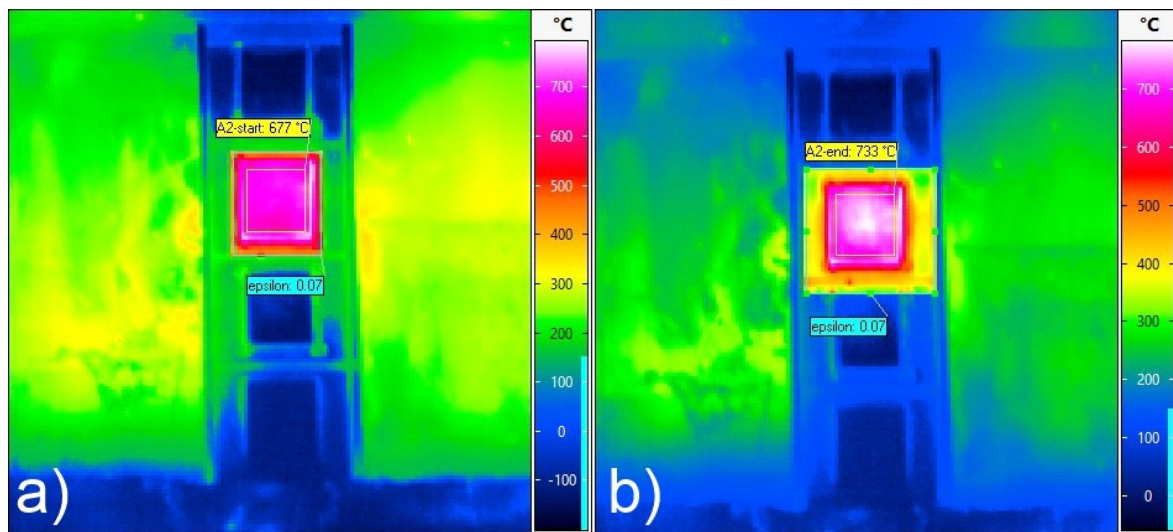

Figure 7: IR images at 10 MW/m² stationary heat load, with an assumed emissivity of 0.07, a) before first transient, b) after 10^5 pulses with 0.14 GW/m². The apparent inhomogeneity of the temperature distribution after the transients is mainly a result of the change in emissivity due to changes in surface morphology.

The available two-color pyrometer, which is in principle hardly affected by emissivity changes, did not provide a clear signal and thus cross-checking the surface temperature and determining the emissivity was not possible. As all samples differ slightly in number and size of their emerging surface features (crack sizes, small pores etc.), also their emissivities will differ. All high-density samples including the recrystallized reference exhibit temperatures (measured by IR with emissivity of 0.07) between 700 °C and 900 °C during combined transient and stationary heat load with no clear trend among samples. The apparent temperatures increased slightly for all samples during the loading due to induced surface modifications as explained before and shown in figure 7.

Table 3: Arithmetic mean roughness of high-density SEBM-W and recrystallized reference W, after polishing and after exposure to 10^5 pulses with 0.14 GW/m².

R_a [µm]	720 W		900 W	
	polished	After 10^5	polished	After 10^5
3000 J/m	0.65	1.97	6.96	7.85
4000 J/m	0.18	1.08	0.14	2.73
5000 J/m	0.28	0.56	**0.12**	**0.95**
Reference	0.15	1.18		

Table 3 lists the mean roughness values of tested samples after polishing and after the 10^5 transient pulses. Except the one sample built at 3000 J/m at 900 W, which exhibited many holes in the surface after polishing, all have very smooth surfaces well below R_a = 1 µm after polishing. The SEBM-W has still few crack clusters, which impact the overall R_a value in a non-trivial manner, and are the main origin for the differences between the reference, and the 4000 J/m and 5000 J/m samples. The discernible trend that samples built at 900 W become slightly rougher under the transient pulses than the ones built at 720 W needs further tests for verification and clarification. The key point here is that the transients led to a roughening on the recrystallized reference and to a similar extent also on the SEBM-W, in particular the one with the best building parameters marked in bold in table 3.
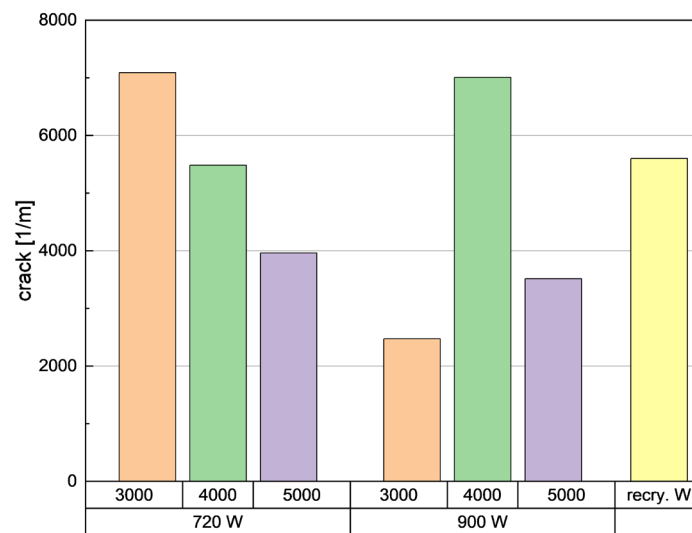

Figure 8: Crack density at the surface after exposure to 10^5 pulses with 0.14 GW/m². It should be noted that the low crack density for the 3000 J/m, 900 W sample is due to many holes at the surface which reduce the effective material area, don't contribute to the crack length but also reduce the stress in their surroundings.

This is consistent when analyzing another damage criterion, the crack density after the exposure. The SEBM-W and the reference develop quite similar crack densities. In particular the ones built with the highest line-energies end up with even slightly lower crack densities. Exemplarily, the change of the surface as response to the transients is shown for the recrystallized reference W and the SEBM-W prepared with the best parameter set (see table 1) in figure 8 and figure 9, respectively. Multiple homogeneously distributed cracks can be observed in case of the recrystallized reference W. In case of the SEBM-W few crack clusters are present from the beginning, which widen slightly during the HHF test. In addition, starting from their tips new cracks develop as well. Only very few cracks form at completely new locations. Thus, despite cracks being present after manufacturing, these potential failure spots do not lead to a shattering of the material, not even necessarily to a higher crack density.
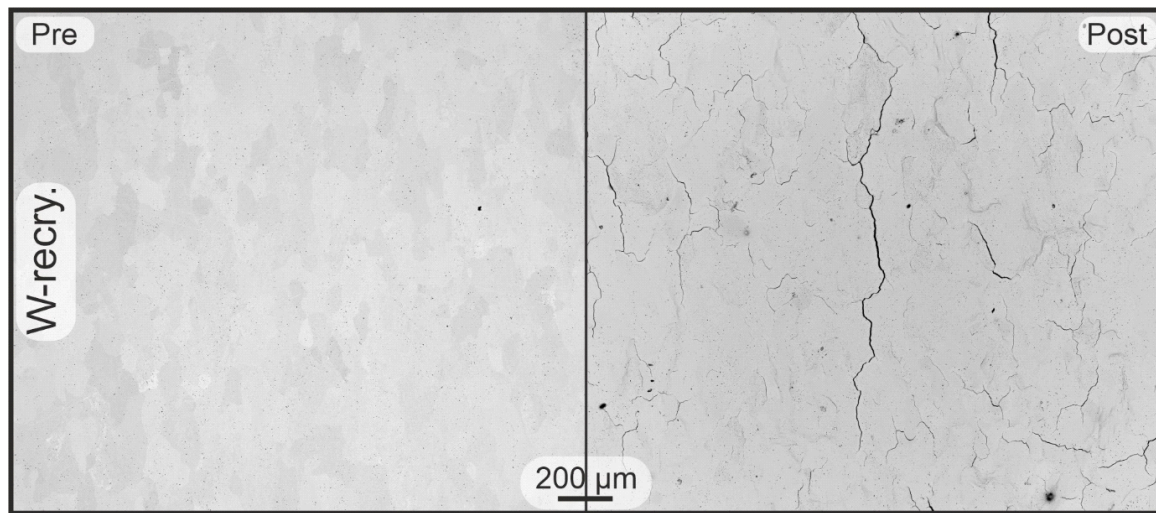
Figure 9: SEM images of the surface of recrystallized W before and after the HHF test. Multiple cracks and roughening can be observed.
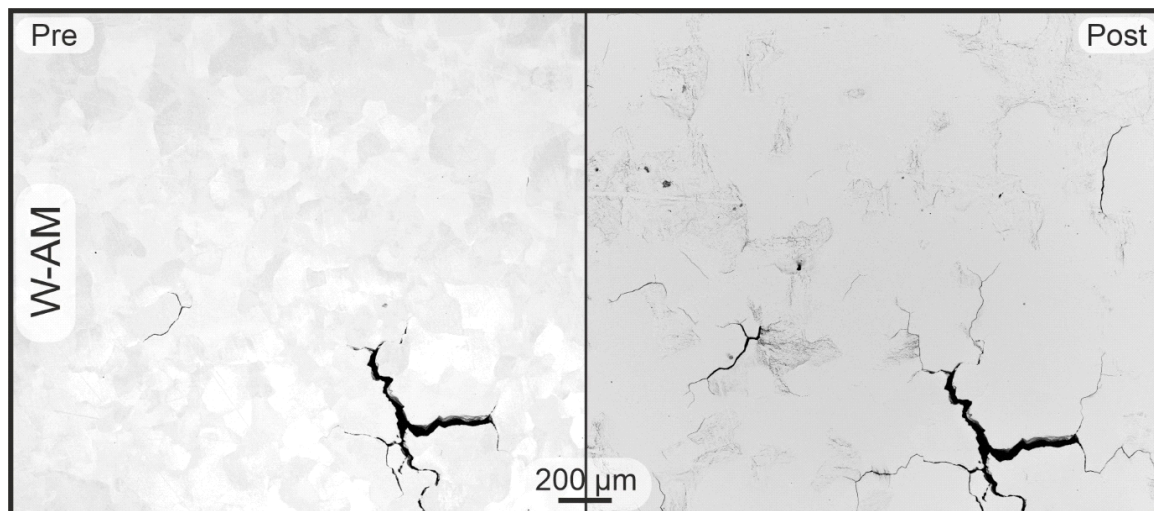

Figure 10: SEM images of the surface of W prepared by AM with the best parameter set (see table 1) before and after the HHF test. Few isolated crack clusters are presented which widen slightly by the thermal loadings. Similar to the recrystallized W, the surface is roughened and few new cracks have formed.

After having demonstrated that very high density can be achieved for SEBM-W, and it offers similar power handling capabilities and damage behavior to standard recrystallized W, the practical benefit AM could have as a manufacturing technique in particular for fusion will be addressed. Figure 11 is a photograph of two monoblocks built by SEBM within the ITER-dimensions regime (28x28x12 mm³ with off-center hole) [18]. As typical for AM a surface finishing step has to be done to achieve a smooth surface. In principle, this is only necessary for the top surface, facing the plasma, which further reduces the necessary effort. As in contrast to other manufacturing techniques no molds or the like are needed, the exact shape, like surface tilt (bevel) or other outer dimensions could be varied individually without cost increase and thus easily adapted and further optimized to the individual location within a future fusion reactor as partly already foreseen [18, 19].
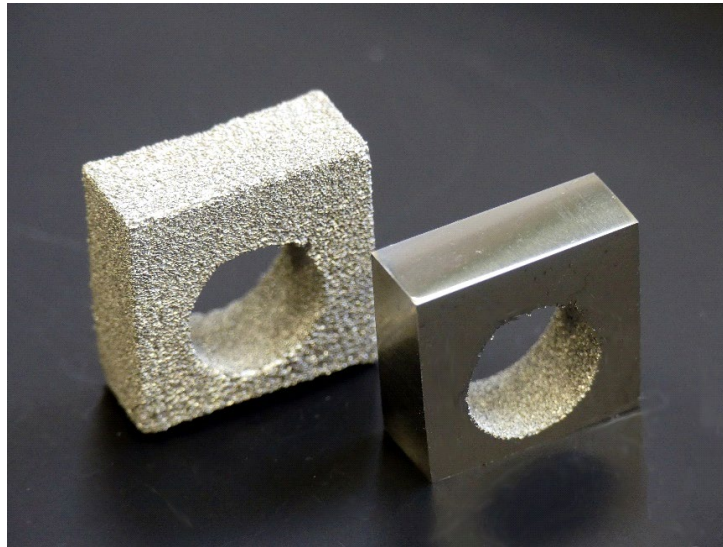
Figure 11: Picture of two SEBM-W ITER-type monoblocks (28x28x12 mm³ with off-center hole). Left after building and right after surface grinding and polishing, illustrating the potential of SEBM for manufacturing near net-shape W-structures.

Conclusion

Within this paper, recent progress in the field of AM of pure W by selective electron beam melting (SEBM) is presented. The influence of building parameters on morphology, density and microstructure is discussed in detail. Three main regions of the resulting SEBM-W with the used line energy could be identified. Nearly crack free material with a relative density of more than 99 % and a hardness like recrystallized W could be built already in this study and directions for further improvements in the search for a crack-free and dense AM-W were identified.

Actively cooled SEBM-W and recrystallized standard W as reference were loaded by an electron beam, simulating ITER-like steady state (10 MW/m²) and transient (10^5 pulses with 0.14 GW/m²) heat loads simultaneously. No macroscopic failure of the SEBM-W occurred despite their preexisting cracks. The power handling capability of high-density SEBM-W and the recrystallized reference W was the same, including a homogenous surface temperature distribution. A slight roughening caused by plastic deformation during the transients could be detected for all samples with no significant difference between the best SEBM-W and the reference. Despite few preexisting cracks in SEBM-W, the crack density after the loading was similar or even slightly lower than in the reference.

These encouraging results demonstrate that AM-W built by SEBM shows similar performance with respect to stationary and transient heat loads as conventional recrystallized tungsten. More sophisticated structures like ITER-type monoblocks have been built successfully as well, proving the flexibility and benefit of AM compared to conventionally fabrication techniques. HHF experiments with more intense thermo shocks also at lower base temperatures are ongoing to further validate the mechanical integrity of the SEBM-W. Also, deuterium plasma exposure experiments are planned in the near future to investigate the impact of the very low but still present internal porosity on the fuel retention of SEBM-W. In future, we will also investigate the potential of SEBM for producing W-alloys to improve the properties and e.g. enhance the strength of the grain boundaries.

Acknowledgement

References

1. Lassner, E.S., W.-D., *Tungsten*. 1st ed. 1999: Springer. 422.
2. Stork, D., et al., *Developing structural, high-heat flux and plasma facing materials for a near-term DEMO fusion power plant: The EU assessment.* Journal of Nuclear Materials, 2014. **455**(1): p. 277-291.
3. BATCHELOR, J.D. and E.L. OLCOTT, *Failure mechanics in dense tungsten alloy rocket nozzles.* Journal of Spacecraft and Rockets, 1964. **1**(6): p. 635-642.
4. Toroi, P., et al., *Experimental investigation on the choice of the tungsten/rhodium anode/filter combination for an amorphous selenium-based digital mammography system.* European Radiology, 2007. **17**(9): p. 2368-2375.
5. Zhang, D., Q. Cai, and J. Liu, *Formation of Nanocrystalline Tungsten by Selective Laser Melting of Tungsten Powder.* Materials and Manufacturing Processes, 2012. **27**(12): p. 1267-1270.
6. Zhou, X., et al., *Balling phenomena in selective laser melted tungsten.* Journal of Materials Processing Technology, 2015. **222**: p. 33-42.
7. Wang, D., et al., *Dense Pure Tungsten Fabricated by Selective Laser Melting.* Applied Sciences, 2017. **7**(4): p. 430.
8. Müller, A.v., et al., *Additive manufacturing of pure tungsten by means of selective laser beam melting with substrate preheating temperatures up to 1000 ∘C.* Nuclear Materials and Energy, 2019. **19**: p. 184-188.
9. Wang, D.-Z., et al., *Cracking Behavior in Additively Manufactured Pure Tungsten.* Acta Metallurgica Sinica (English Letters), 2019. **32**(1): p. 127-135.
10. Körner, C., *Additive manufacturing of metallic components by selective electron beam melting — a review.* International Materials Reviews, 2016. **61**(5): p. 361-377.
11. v. Müller, A., et al., *Microstructural investigations of tungsten manufactured by means of laser beam melting*. 2016.
12. Tan, C., et al., *Selective laser melting of high-performance pure tungsten: parameter design, densification behavior and mechanical properties.* Science and Technology of Advanced Materials, 2018. **19**(1): p. 370-380.
13. Majerus, P., et al., *The new electron beam test facility JUDITH II for high heat flux experiments on plasma facing components.* Fusion Engineering and Design, 2005. **75-79**: p. 365-369.
14. Loewenhoff, T., et al., *Experimental simulation of Edge Localised Modes using focused electron beams – features of a circular load pattern.* Journal of Nuclear Materials, 2011. **415**(1, Supplement): p. S51-S54.
15. Wang, X., et al., *Densification of W–Ni–Fe powders using laser sintering.* International Journal of Refractory Metals and Hard Materials, 2016. **56**(Supplement C): p. 145-150.
16. Regenfuss, P., et al., *Principles of laser micro sintering.* Rapid Prototyping Journal, 2007. **13**(4): p. 204-212.
17. Alfonso Lopez, A., et al., *Thermal stability of a highly-deformed warm-rolled tungsten plate in the temperature range 1100–1250 °C.* Fusion Engineering and Design, 2015. **98-99**: p. 1924-1928.
18. Pitts, R.A., et al., *Physics basis and design of the ITER plasma-facing components.* Journal of Nuclear Materials, 2011. **415**(1, Supplement): p. S957-S964.
19. Pitts, R.A., et al., *Physics conclusions in support of ITER W divertor monoblock shaping.* Nuclear Materials and Energy, 2017. **12**: p. 60-74.